Pore size tuning of bis(triethoxysilyl)propane (BTESP)-derived membrane for gas separation: Effects of the acid molar ratio in the sol and of the calcination temperature

Ryota Inoue,[a] Masakoto Kanezashi,[a,*] Hiroki Nagasawa,[a] Kazuki Yamamoto,[b] Takahiro Gunji,[b] and Toshinori Tsuru

[a] Department of Chemical Engineering, Graduate school of Engineering, Hiroshima University, 1-4-1 Kagamiyama, Higashi-Hiroshima 739-8527, Japan

[b] Department of Pure and Applied Chemistry, Tokyo University of Science, Noda, 278-8510, Japan

*Corresponding author: kanezashi@hiroshima-u.ac.jp

Abstract

Bis(triethoxysilyl)propane (BTESP) is a bridged-type organoalkoxysilane with a Si-C_3H_6-Si bond. It was utilized for membrane fabrication via a sol-gel method to achieve high permselectivity for large molecules. Membrane fabrication parameters such as the acid molar ratio (AR) in the sol and calcination temperature were evaluated for their effect on the network pore size and on gas permeation properties, as evaluated by the molecular size dependence (0.26-0.55 nm) and temperature dependence (50-200 °C) of gas permeance. BTESP membranes with different ARs (10^{-1}, 10^{0}, and 10) showed H_2/N_2 and H_2/CF_4 selectivities of 20-30 and 640-32000, respectively. As AR was increased, each gas permeance also increased, but H_2 selectivity that corresponds to network pore size was decreased. FT-IR analysis indicated that the density of the Si-OH groups (Si-OH/Si-O-Si) of unfired gels was decreased with a higher AR, so that condensation of the Si-OH groups during the calcination process formed a dense network structure in the case of

BTESP membranes with a low AR (10^{-1}). Calcination temperature also affected the network structure of BTESP membranes. BTESP membranes calcined at different temperatures (350, 450, and 600 ºC) showed H_2/N_2 and H_2/CF_4 selectivities of 10-30 and 410-32000, respectively. A BTESP membrane calcined at high temperature (600 ºC) showed loose networks since the linking units derived from BTESP were decomposed at temperatures above 500 ºC, which resulted in the formation of methyl groups. In conclusion, the AR in a sol is suitable for tuning small pore sizes, while calcination temperature as a membrane fabrication parameter offers the advantage of controllability for loose network structures.

Keywords: Organosilica; Membrane; Gas separation; Pore size; Activation energy

1. Introduction

Porous silica membranes have amorphous structures with high thermal and chemical stabilities, and these membranes are fabricated via chemical vapor deposition (CVD) [1-3] and/or sol-gel [4-6] methods. Tetraethoxysilane (TEOS)-derived conventional silica membranes with an average pore size of 0.3-0.4 nm show high selectivity for small gases such as H_2 (0.289 nm) /N_2 (0.364 nm) or H_2/CO_2 (0.33 nm) [7-13]; the pore sizes of conventional silica membranes are too small for H_2/hydrocarbon or C3-C4 hydrocarbons separation, however, so that the development of silica membranes with a loose network structure is preferable.

There are many reports on the tuning of silica network structures and the improvement of hydrothermal stability by using organic/inorganic silica precursors [14-28]. In particular, bridged-type organosilica membranes have a loose network structure because organic linking units between the Si atoms assume the role of a spacer, and the Si atomic distance can remain large [19, 20]. The effects that a spacer species of bridged-organoalkoxysilane exerts on microporous structures and gas permeation properties have recently been discussed [29-36]. Organosilica with short linking units (C_nH_{2n}, n = 1, 2) creates a rigid silica network, and membranes with a microporous structure and molecular sieving properties have dominant gas permeation properties similar to conventional silica membranes. On the other hand, long linking units (C_nH_{2n}, n = 3-10) such as alkyl chains make the silica network more flexible and the permeable pores were blocked at 77 K, which demonstrated a nonporous structure. Thus, a solution-diffusion mechanism that is based on the thermal vibrations of alkyl chains [37, 38] dominates the gas permeation properties of organosilica membranes.

In terms of H_2/C_3H_8 separation, organosilica membranes with C1-C3 alkyl chains

have achieved the upper bounds of the trade-off between H_2 permeance and H_2/C_3H_8 selectivity [39]. It should be noted that bis(triethoxysilyl)propane (BTESP)-derived membranes with a propylene group as the linking unit have shown a high H_2 permeance of 2×10^{-6} mol m^{-2} s^{-1} Pa^{-1} and an H_2/C_3H_8 selectivity of 6000. This indicates that BTESP membranes have a moderately loose network structure, which makes them suitable for the separation of H_2 from large molecules, but the performance of these membranes is yet to be optimized.

The membrane fabrication process has been used to control the silica network structure. In sol-gel processing, the H_2O/Si [40,41] and HCl/Si [42,43] ratio in a sol can facilitate/inhibit hydrolysis and condensation of Si-OEt and Si-OH groups for network formation and can make the membrane pore size small/large. In the calcination process, pendant-type organosilica membranes can form large pores via the decomposition of a pendant group under an air atmosphere [44-46], while in the case of bridged-type organosilica, a densification of the network structure occurs at high temperature (> 300 ^oC) via the pyrolysis of a bridged alkyl chain and the forming of a SiO_2-like structure [47]. However, it is unclear how membrane fabrication conditions affect either the network structure or the gas permeation properties of BTESP membranes.

In the present study, we evaluated the effect that the HCl/Si (acid molar ratio, AR) in a sol and the calcination temperature exerts on network pore size and on the gas permeation properties of BTESP membranes. BTESP-derived sols were prepared with ARs = 10^{-2}, 10^{-1}, 10^0, and 10, and calcination temperatures were controlled at 350-600 ^oC under a N_2 atmosphere. The chemical and microporous structure were evaluated by Fourier transform infrared (FT-IR) and N_2 adsorption, respectively. The effect of calcination temperature on the C/Si ratio and the state of carbon in the BTESP network

was evaluated by thermogravimetric-mass spectrometric (TG-MS) analysis and nuclear magnetic resonance (NMR). We measured the molecular size and temperature dependence of gas permeance for BTESP membranes and evaluated the network size via gas selectivity and activation energy.

2. Experimental

2.1 Preparation of BTESP sol and membrane fabrication

BTESP is not commercially available, so we synthesized a BTESP monomer in our laboratory by following a procedure found in the literature [38]. The BTESP sols were prepared by hydrolysis and condensation. BTESP, water (H_2O/BTESP=200), and HCl (HCl/BTESP=10^{-2}-10) were added to ethanol (>99.5 vol%) in this order, and 5 wt% BTESP sols were prepared by stirring the solution (500 rpm) for an hour at 50 °C. The weight-based compositions of the prepared BTESP sols are summarized in Table S1.

BTESP membranes were fabricated on α-alumina porous tubes (Nikkato Ltd, Japan) with an average pore size of 1 μm. The membranes were composed of three layers: a particle layer, an intermediate layer, and a separation layer. Each layer was formed by wipe-coating with a cloth and calcination. A particle layer with a pore size of 0.9 μm was formed by α-alumina particles (particle size: 1-2 and 0.2 μm) mixed with a SiO_2-ZrO_2 sol and calcined at 550-700 °C under an air atmosphere for 10 min. The intermediate layer had an average pore size of approximately 0.6 nm and was formed in the same manner using a SiO_2-ZrO_2 sol (particle size: 5-100 nm) diluted to 0.5wt% using distilled water. Then, the BTESP layer was formed with a coating of 0.5wt% BTESP sols followed by calcination at 350-700 °C (N_2 atmosphere for 10 min). The thickness of the BTESP separation layer was difficult to identify because there was no change in the thickness

after coating the BTESP sol onto the SiO_2-ZrO_2 intermediate layer, but the uniform nature of the BTESP separation layer was confirmed from the SEM images of the surface, as shown in Fig. S1.

2.2 Characterization of BTESP-derived films and gels

The FT-IR spectra of BTESP films coated onto KBr plates were measured utilizing a FT-IR spectrometer (FT/IR-4100, JASCO, Japan). BTESP sols (5 wt%) were deposited on KBr plates by spin-coating at 5000 rpm for 30 s, and prior to calcination the BTESP films were obtained by drying at room temperature. The dried film was then calcined at 350 ºC under a N_2 atmosphere to observe the effect of calcination. BTESP gel powders were prepared by drying and gelation at 40 ºC with calcination at 350-800 ºC under a N_2 atmosphere. TG-MS (TGA-DTA-PIMS 410/S, Rigaku, Japan) was used for thermogravimetry analysis of evolved gas from BTESP powders, and the chemical structures of the samples were analyzed via nuclear magnetic resonance (NMR, Varian 600PS solid NMR spectrometer). Solid-state ^{29}Si MAS-NMR was measured at 119.2 MHz setting the recycle delay at 70 s for 400 scans. We use a 3-(trimethylsilyl)propionic-2,2,3,3-d_4 acid sodium salt as the reference for the peak position. ^{13}C CP MAS-NMR measurements were conducted at 150.9 MHz by ^{13}C-^{1}H dipolar couplings, and the spectra was obtained by setting the recycle delay at 70 s for 360 scans. The peak position was referenced using hexamethylbenzene.

2.3 Single-gas permeation measurement

Fig. 1 shows a schematic diagram of the single-gas permeation device. Single gases (He, H_2, CO_2, N_2, CH_4, CF_4, SF_6) were supplied to the outside of the membrane, and the

gas permeation temperature was controlled at 50-200 ºC. Upstream and downstream pressure was maintained at 200-300 kPa and atmospheric pressure, respectively. The permeation rate was measured by utilizing a soap film flow meter (SF-U, Horiba Ltd, Japan), and the measurement error for each permeance was less than 5%.

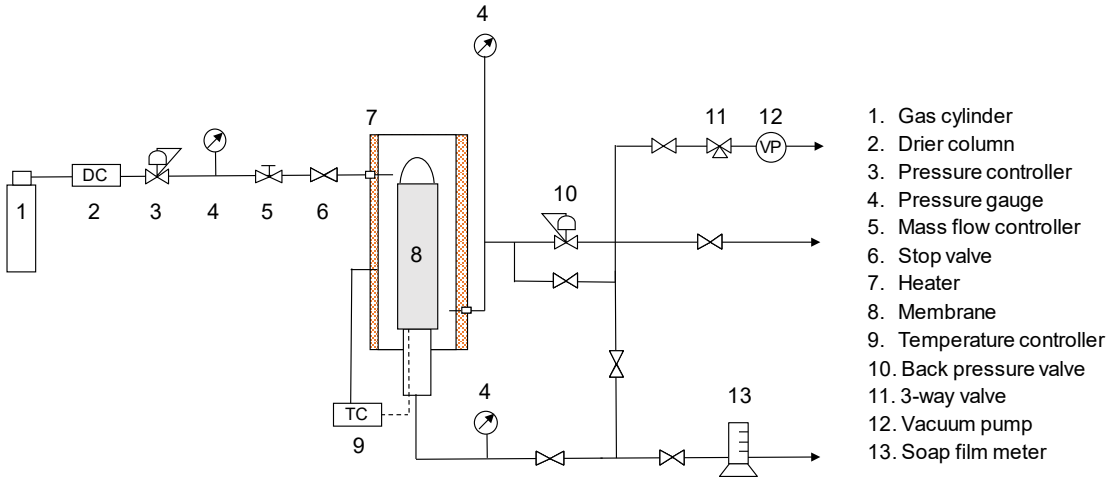

Fig. 1 Schematic diagram of the experimental apparatus for single-permeation measurement.

3. Results and discussion

3.1 Effect of the acid molar ratio in the sol on the physicochemical properties and membrane permeation properties of BTESP

Fig. 2 (a) shows the FT-IR spectra in the range of 600-3200 cm^{-1} for BTESP films with different acid molar ratios of the sol (ARs = 10^{-2}, 10^{-1}, 10^{0}, and 10) before calcination. Peaks centered at 1000-1100 cm^{-1} assigned to Si-O-Si asymmetric stretching vibrations [48] were detected in all samples, and indicated that a silica network had formed during the hydrolysis of Si-OEt and the condensation of Si-OH. It was apparent that the ethoxy

groups were completely hydrolyzed even with AR values as small as 10^{-2}, due to the absence of -CH_3 peaks (2974 cm^{-1} [49]) originating from Si-OEt, which was detected in the FT-IR spectra of the BTESP precursor, as shown in Fig. S2. The detected peaks at 1270 cm^{-1} and 2932 cm^{-1} were attributed to the silsesquioxane bonding (SiC) [50,51] and C-H_x stretching vibrations of -CH_2- fragments [52], respectively; thus, it was suggested that the linking units for BTESP (Si-C_3H_6-Si) were retained in the silica networks regardless of AR.

After calcination at 350 °C under N_2, as shown in Fig. 2 (b), the peak height assigned to SiOH (890 cm^{-1} [53]) was clearly decreased by comparison with that before calcination because of condensation during the calcination process, which led to an increase in the peak height of Si-O-Si centered at 1030 cm^{-1}. No changes were confirmed in the peaks of the Si-C and -CH_2- groups that originated from the linking units. It should be noted that FT-IR analysis for BTESP films before/after calcination was performed on the same film for each acid molar ratio. Also, more than 2 films were used for each AR analysis to confirm the reproducibility.

The density of the Si-OH groups with different acid molar ratios in the sol used to produce the BTESP film was assessed via the Si-OH/Si-O-Si peak area ratios derived from Fig. 2. Fig. 3 shows the Si-OH/Si-O-Si peak area ratios for BTESP films as a function of the acid molar ratio in the sol. The Si-OH/Si-O-Si peak area ratios for the films before calcination were greatly decreased with increases in the AR in the sol, suggesting that condensation proceeded at a higher degree with a higher AR. In contrast, the peak area ratios for the films after calcination at 350 °C were comparable, and were almost independent of the AR. This indicates that BTESP-derived networks with different ARs in the sol have a comparable density of silanol groups after calcination at 350 °C,

and that the degree of condensation during the calcination process is low for a sol with a high AR. A similar trend was confirmed in BTESE-derived membranes with -C_2H_4- linking units [43], suggesting that the effect of the AR on the silica network structure is common among organosilica membranes.

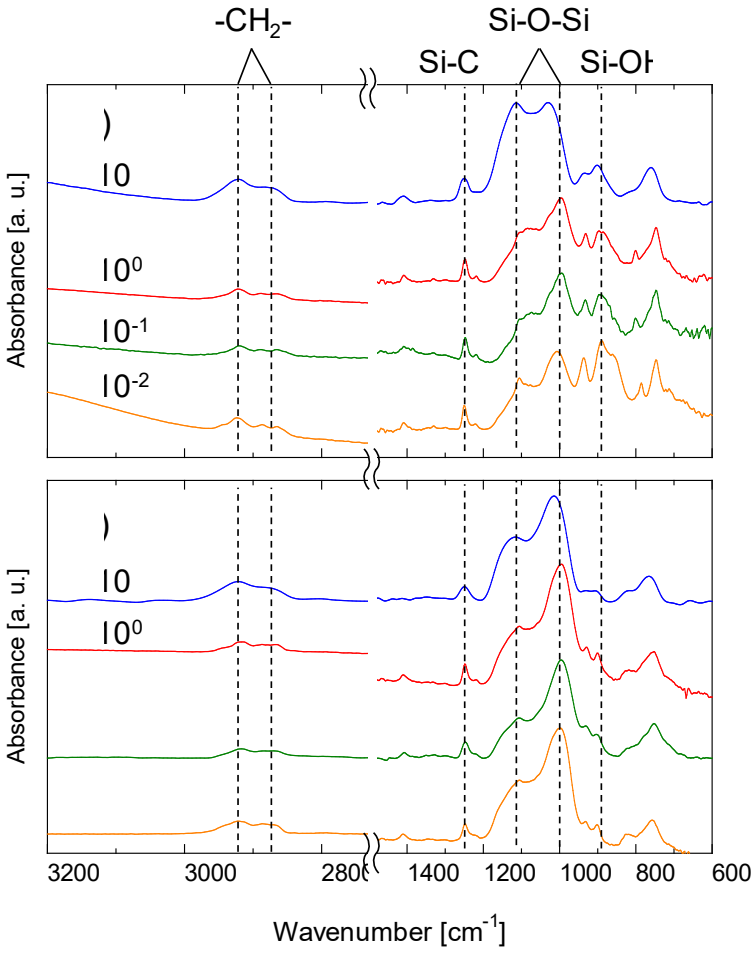

Fig. 2 FT-IR spectra in the range of 600-3200 cm^{-1} for BTESP-derived films prepared with ARs = 10^{-2}, 10^{-1}, 10^{0}, and 10 ((a) before calcination, (b) after calcination at 350 °C under N_2).

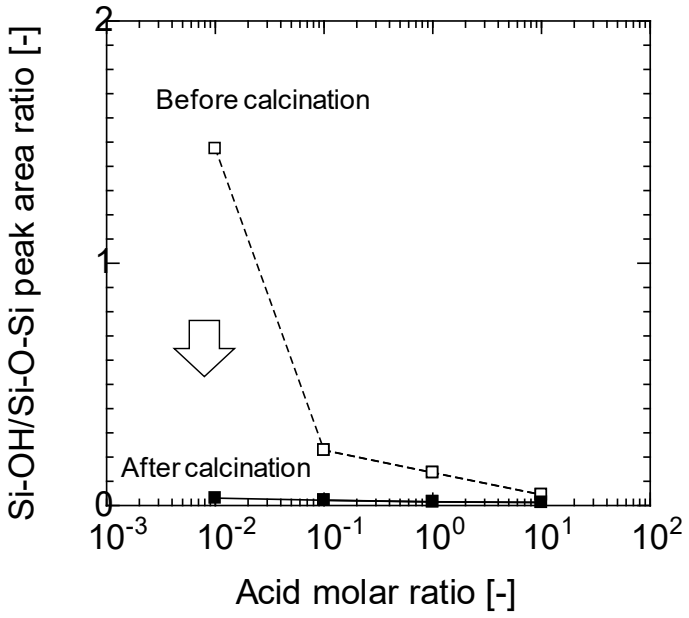

Fig. 3 Si–OH/Si–O–Si peak area ratios for BTESP films as a function of the acid molar ratio in the sol (open symbols: before calcination, closed symbols: after calcination at 350 ^{o}C under N_2).

The network pore size of the BTESP membrane was evaluated according to the molecular size dependence of gas permeance at 200 ^{o}C where molecular sieving is dominant during permeation due to the diminished effect of adsorption. Fig. 4 shows the molecular size dependence of gas permeance (a) and dimensionless permeance normalized by He permeance (b) at 200 ^{o}C for BTESP membranes with ARs = 10^{-2}, 10^{-1}, 10^{0}, and 10 when calcined at 350 ^{o}C. In Fig. 4 (b), each measure of permeance was divided by He permeance, corresponding to gas X/He selectivity, to discuss the average pore size of each BTESP membrane. In the present study, to minimize the effect of intermediate layer on membrane performance, BTESP membranes were fabricated on intermediate layers that had approximately the same average pore size and gas permeance,

as shown in Fig. S3. All the BTESP membranes showed H_2 permeance higher than 1×10^{-7} mol m^{-2} s^{-1} Pa^{-1}, and the BTESP membrane with an AR = 10^{-1} showed selectivity for H_2/N_2 of 30 and for H_2/CF_4 of 32000. Each gas permeance was increased with increases in the AR, while H_2 selectivity, which corresponds to network pore size, was decreased with a higher AR. For example, the membrane with an AR = 10 showed H_2/N_2 selectivity of 20 and H_2/CF_4 selectivity of 640. H_2/CF_4 selectivity of the membrane with an AR = 10^{-2} was lower than that with an AR = 10^{-1} despite the latter value being a lower AR. These results show that a BTESP-derived loose network structure can be formed by using a sol with a high AR.

Fig. 5 features a schematic image showing the effect that the acid molar ratio has on the formation of the BTESP network structure before/after calcination. The important point is that the number of Si-OH groups in the silica network before calcination is dependent on the AR in the sol. The number of Si-OH groups before calcination is increased with a lower AR in the sol, as shown in Fig. 3, which indicates that a large number of Si-OH groups are available to be condensed via calcination. In the calcination process, a dense network structure is formed by utilizing a sol with a low AR because the calcination process creates small pores via the condensation of closely aligned silanol groups, which are abundant in the sol. By contrast, a sol with a high AR has fewer silanol groups, which creates a loose network structure due to a slight change in the network structure during the calcination process [43].

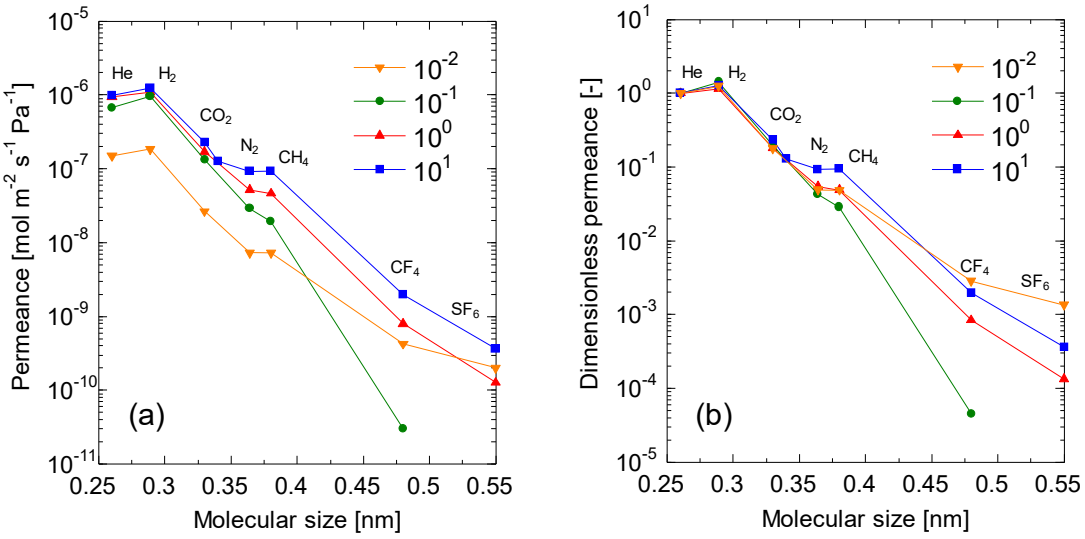

Fig. 4 Molecular size dependence of gas permeance (a) and dimensionless permeance based on He permeance (b) at 200 °C for BTESP membranes prepared with ARs = 10^{-2}, 10^{-1}, 10^{0}, and 10 (calcined at 350 °C under N_2).

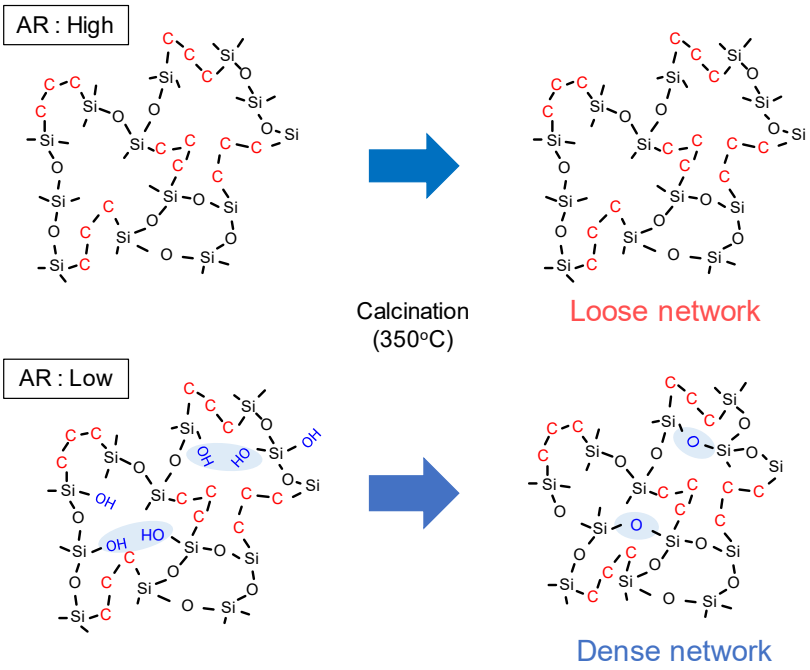

Fig. 5 Schematic image of the formation of the BTESP network structure before/after calcination: effect of the acid molar ratio on BTESP networks.

H_2/CF_4 selectivity is reportedly correlated with H_2/C3 hydrocarbon selectivity because the molecular size of CF_4 (0.48 nm) is comparable to that of both propane (0.50 nm) and propylene (0.47 nm). Fig. 6 shows the H_2/CF_4 selectivities for bis(triethoxysilyl)methane (BTESM) [29,38], BTESE [38,43,47], and BTESP-derived membranes as a function of H_2 permeance at 200 °C. In order to confirm the reproducibility of membrane with different ARs, in the present study, at least 2 membranes for each AR was fabricated and each point in Fig. 6 corresponds to one membrane. Membranes with high permeance generally show low selectivity, and the broken lines in the figure show the trade-off relationships for BTESM and BTESE membranes. The H_2 permeance of BTESP membranes was significantly increased from 6.3×10^{-7} to 4.6×10^{-6} mol m^{-2} s^{-1} Pa^{-1} and the H_2/CF_4 selectivity was decreased from 32000 to 200 with an increase in the AR in the sol of from 10^{-1} to 10. Based on the results of N_2 adsorption at 77 K (Fig. S4), the total pore volume of BTESP powders was large with an increase in the AR, which demonstrated that an increase in gas permeance is related to a larger effective area for gas permeation as well as to the effective enlargement of the network pore sizes. The BTESP membrane with an AR = 10^{-1} showed the highest H_2/CF_4 selectivity of 32000, which was beyond the trade-off relationship.

H_2/CF_4 selectivity of the membrane with an AR = 10^{-2} was lower than that with an AR=10^{-1} despite the latter value being a lower AR. Although a lower AR creates a denser network structure, the high degree of condensation during the calcination process allowed

large network pores to simultaneously form, which promoted the permeation of CF_4. According to the above results, the BTESP membrane with an AR = 10^{-1} proved to be suitable for H_2/C3 hydrocarbon separation. Binary separation performance at 200 °C for a BTESP membrane with AR=10^{-1} was conducted and the results appear in Fig. S5. The permeance of both H_2 and C_3H_8 was independent of the mole fraction of C_3H_8 in feed, and the H_2/C_3H_8 permeance ratio was approximately the same as that obtained by single-gas permeation (2900), due to a negligible adsorption of the adsorptive molecules at temperatures above 200 °C.

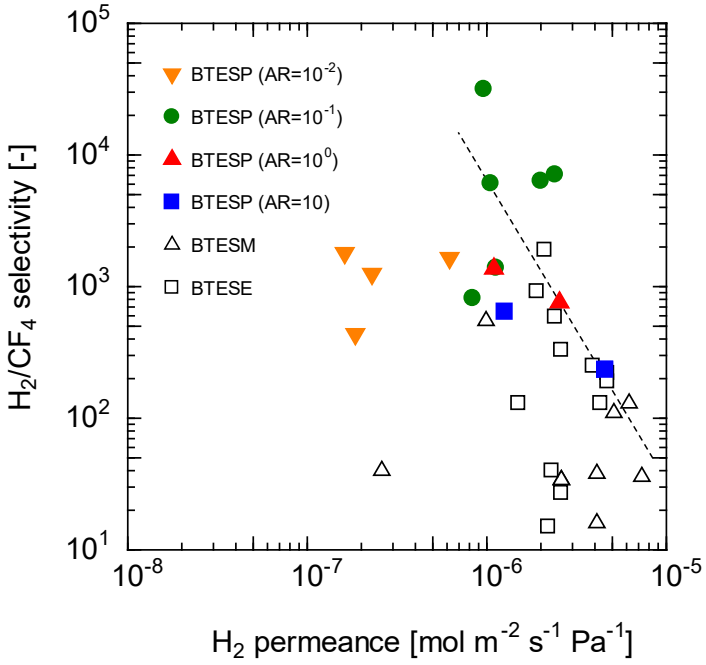

Fig. 6 H_2/CF_4 selectivity for BTESM [29,38], BTESE [38,43,47], and BTESP-derived membranes as a function of H_2 permeance at 200 °C.

3.2 Effect of calcination temperature on the decomposition properties of linking units and on the network pore sizes of BTESP membranes

The thermal stability and decomposition properties of the linking units were evaluated via TG-MS measurement under a He atmosphere. BTESP gel prepared with an AR=10^{-1} was heated at 200 ºC for 120 min to remove any adsorbed water, and then heated to 1000 ºC at a rate of 10 ºC min^{-1}. Fig. 7 shows the TG curves and mass signals for BTESP gels prepared with an AR = 10^{-1} under a He atmosphere. The relative weight was decreased by 3% for temperatures ranging from 200-500 ºC. This was caused by desorption of the adsorbed water and condensation of the Si-OH groups [54-56]. A significant weight loss (5%) was observed for temperatures ranging from 500-700 ºC where mass peaks derived from methane and hydrogen were detected, and, therefore, the propylene linking units of BTESP were considered to be thermally decomposed. Hence, calcination temperature is considered an important parameter for controlling the C/Si ratio and decomposition properties of linking units within the BTESP network structure.

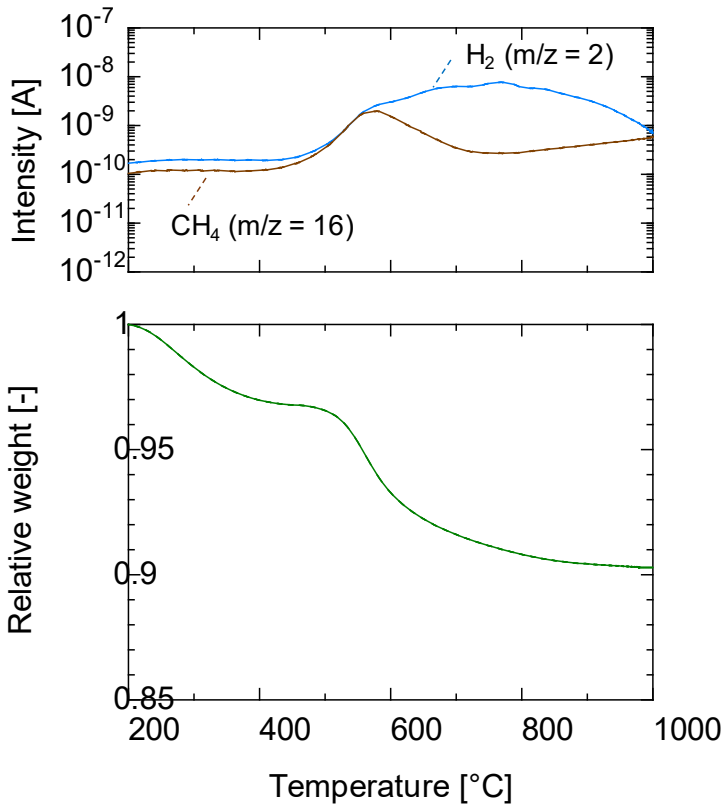

Fig. 7 TG curve and mass signals of BTESP gels prepared with an AR = 10^{-1} under a He atmosphere.

Fig. 8 shows the ^{29}Si MAS-NMR spectra of BTESP gel powders (AR=10^{-1}) calcined at different temperatures (350, 600, and 800 °C) under a N_2 atmosphere. These powders were prepared for analyzing BTESP-derived chemical structures over the wide range of the calcination temperature including that before/after the thermal decomposition. A T^2 unit (-55 ppm) with a Si-OH group was detected in a powder calcined at 350 °C, but the peak was shifted to that of a T^3 unit (-65 ppm) that corresponded to Si-O-Si [57] when calcined at 600 °C. A deconvolution of the T unit (T^2+T^3) was conducted and the results appear in Fig. S6 and Table 1. The BTESP powder calcined at 350 °C showed T^2/T_{total}

peak area ratio of 0.75. As the calcination temperature increased, the peak area ratio was decreased to 0.02 in the powder calcined at 800 °C. This indicates that condensation of the Si-OH group had proceeded under the high calcination temperature.

The Q unit (Q^3+Q^4) derived from SiO_2 was increased with a higher calcination temperature, so that a rearrangement of siloxane bonds had occurred due to pyrolysis of the linking units under high calcination temperatures [58]. Also, the T/(T+Q) peak area ratios for BTESP powders calcined at different temperatures are summarized in Table 1. The peak area ratio of the powder calcined at 350 °C was 1.00, which indicated that the propylene groups between the Si atoms had completely remained in the BTESP network structure. As the calcination temperature increased, the T peak area ratio was decreased, but the powder calcined at 800 °C continued to show a high T peak area ratio of 0.84.

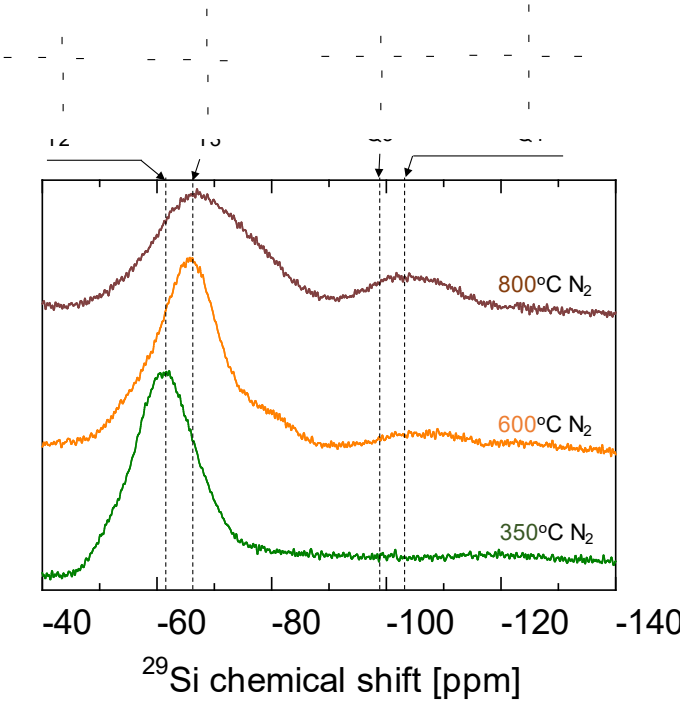

Fig. 8 ^{29}Si MAS-NMR spectra of BTESP-derived gels (AR = 10^{-1}) calcined at different

temperatures under a N_2 atmosphere.

Table 1 Peak area ratio of BTESP gels calcined at different temperatures under a N_2 atmosphere.

Peak area ratio [-]	Calcination temperature [°C]		
	350	600	800
T^2/T_{total}	0.75	0.20	0.02
$T_{total}/(Q_{total}+T_{total})$	1.00	0.91	0.84

To analyze the effect of calcination temperature on the carbon status of BTESP, the ^{13}C CP MAS-NMR spectra of the gel powders (AR=10^{-1}) calcined at 350, 600, and 800 °C were measured and the results appear in Fig. 9. Assignment of the chemical shift of the propylene group in BTESP solid-state ^{13}C NMR was performed based on assignment of the BTESP precursor, as shown in Fig. S7. A peak at 13 and 19 ppm assigned to the propylene group was detected in the powder calcined at 350 °C, which is consistent with the results of ^{29}Si-NMR (Fig. 8). In the powder calcined at 600 °C, three peaks were detected due to pyrolysis of the propylene groups. These peaks were assigned to the propylene, ethylene (6 ppm), and methylene (-1 ppm) groups, respectively. This indicates that a BTESP network structure calcined at 600 °C has various carbon structures. The peaks derived from the bridged alkyl chain between the Si atoms had approximately disappeared, and a peak assigned to the methyl group (-6 ppm) was only detected [59-61] in the powder calcined at 800 °C.

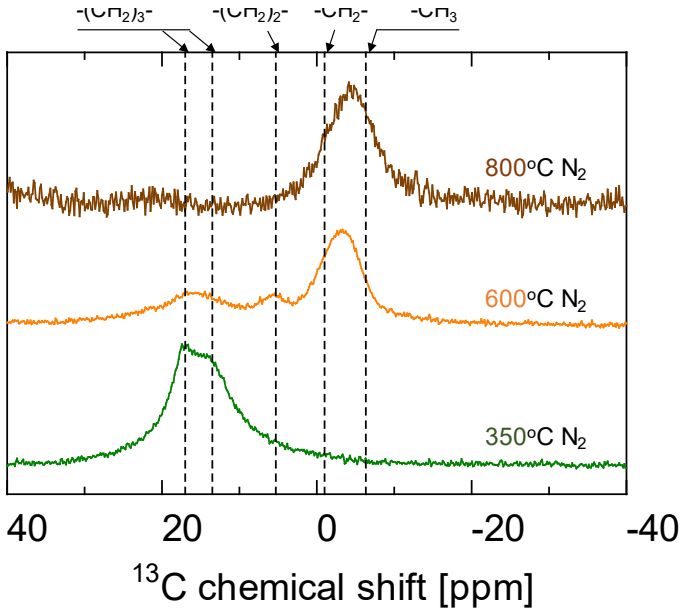

Fig. 9 ^{13}C CP MAS-NMR spectra of BTESP-derived gels (AR = 10^{-1}) calcined at different temperatures under a N_2 atmosphere.

Fig. 10 shows the molecular size dependence of gas permeance (a) and dimensionless permeance based on He permeance (b) at 200 °C for BTESP membranes (AR = 10^{-1}) calcined at different temperatures (350, 450, and 600 °C). The BTESP membrane calcined at 350 °C showed a H_2/N_2 selectivity of 30 and a H_2/CF_4 selectivity of 32000; the H_2/N_2 selectivity was slightly increased by calcination at 450 °C. This indicates that condensation of the Si-OH groups in the network structure had occurred at 450 °C, and the network pore size was decreased. A membrane calcined at 600 °C showed a relatively high N_2 permeance of 5.5×10^{-7} mol m^{-2} s^{-1} Pa^{-1} with low H_2/N_2 and high N_2/SF_6 selectivities of 11 and 780, compared with those of the membrane calcined at 350 and 450 °C, respectively. This indicates that the BTESP membrane calcined at 600 °C had a

moderately loose network structure. In this case, molecular sieving for small gases such as H_2 and N_2 was decreased, resulting in decreased H_2/N_2 selectivity. Since large molecules such as CF_4 and SF_6 cannot permeate a moderately loose network structure, this showed low H_2/N_2 selectivity that was nonetheless highly selective for N_2 over SF_6 molecules. Based on the results of the ^{13}C CP MAS-NMR spectra of BTESP-derived gels when calcined at 600 ºC, a moderately loose network was formed via a change in the state of the carbon to methyl groups.

Fig. 11 features a schematic image of the formation of a BTESP network structure (AR = 10^{-1}) and the effect of calcination temperature on BTESP network structures. Calcination temperature acts on the progression of the condensation of Si-OH groups in the network and promotes pyrolysis of the linking units. In the case of low calcination temperature (350-450 ºC), however, the condensation occurs without pyrolysis of the linking units, so that a dense network structure can be formed. On the other hand, when a BTESP membrane is fabricated at high calcination temperatures (500-600 ºC), the thermal decomposition of propylene groups forms methyl and methylene groups in the networks (condensation is completed according to the TG curve), and a loose network structure is formed.

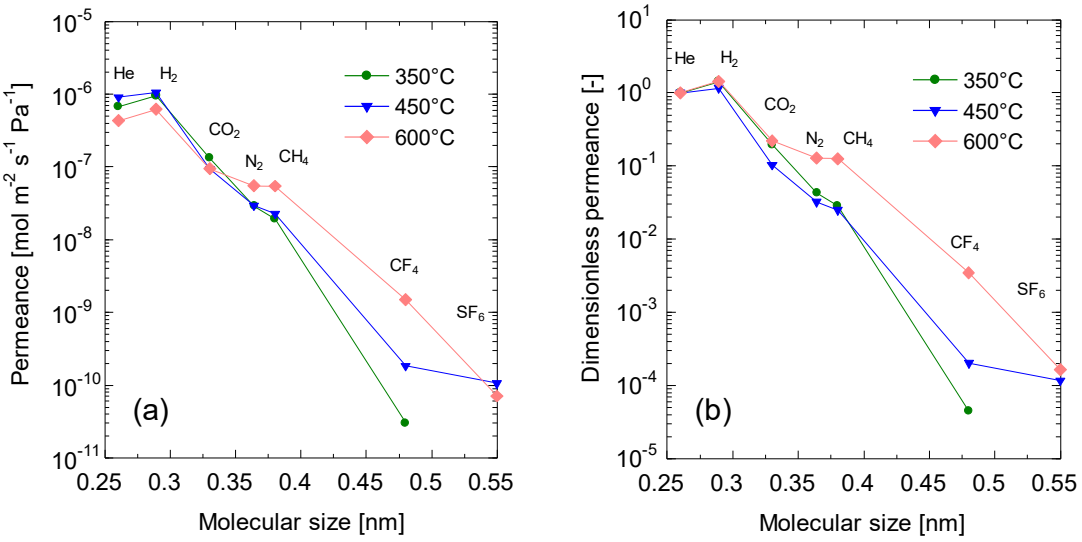

Fig. 10 Molecular size dependence of gas permeance (a) and dimensionless permeance based on He permeance (b) at 200 °C for BTESP membranes calcined at 350-600 °C under N_2.

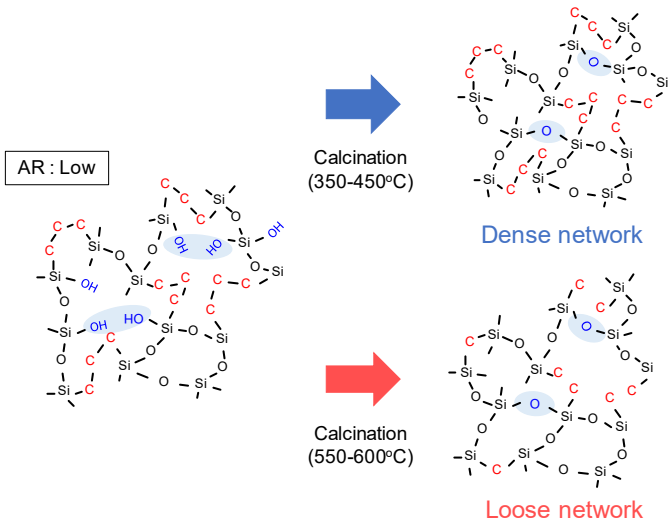

Fig. 11 Schematic image of the formation of a BTESP network structure (AR = 10^{-1}), and

the effect of calcination temperature on BTESP network structures.

3.3 Evaluation of a BTESP network by activation energy and He selectivity

Fig. 12 (a) shows the temperature dependence (50-200 ºC) of gas permeance for a BTESP membrane (AR = 10^{-1}) calcined at 350 ºC. The gas permeance of He and H_2 showed an increasing trend with increases in temperature, and N_2 and CH_4 showed gas permeation that was based on activated diffusion. On the other hand, CO_2, the most adsorptive molecule, showed surface diffusion due to a strong affinity for SiO_2.

Fig. 12 (b) shows the temperature dependence (50-200 ºC) of gas permeance for a BTESP membrane (AR = 10^{-1}) calcined at 600 ºC. The gas permeance of neither He nor H_2 depended on temperature, and that of N_2, CH_4, CF_4, and SF_6 were decreased with increases in temperature (Knudsen diffusion). Large molecules such as CF_4, and SF_6 are considered to permeate the loose network pores created by the pyrolysis of propylene groups. No change was observed in the permeation properties of CO_2 molecules after calcination.

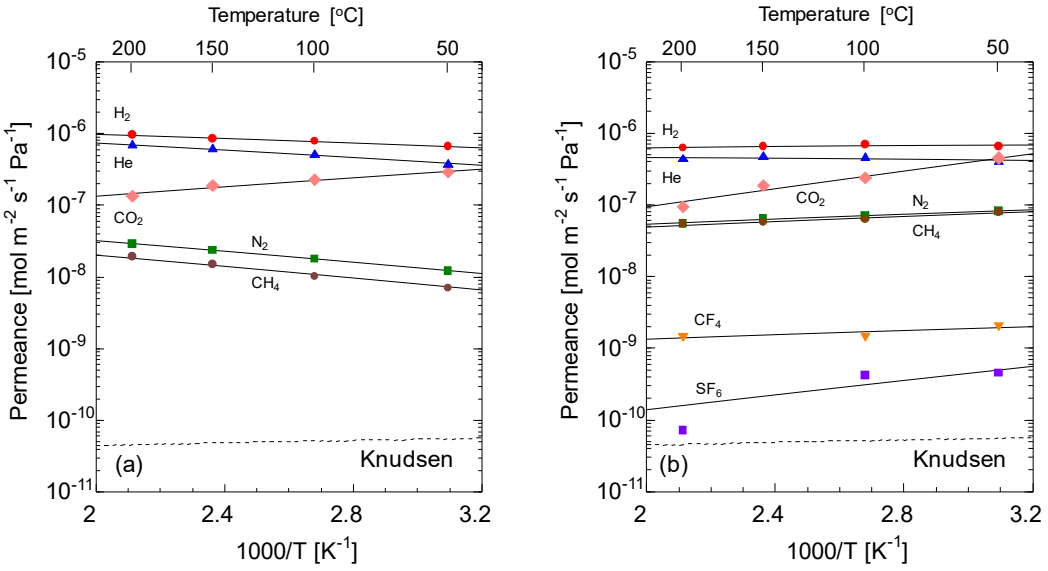

Fig. 12 Temperature dependence of gas permeance for a BTESP membrane (AR = 10^{-1}) calcined at 350 °C (a) and that calcined at 600 °C (b).

The effects of calcination temperature on the gas permeation properties and network structures for the BTESP membranes (AR=10^{-1}) were compared with those of microporous SiO_2-based membranes. Fig. 13 shows He/H_2 selectivity (a), He/N_2 selectivity (b) at 200 °C, and activation energy for He permeation (c) as a function of calcination temperature for BTESP, BTESE [47], and SiO_2 (TEOS) [62] membranes. Small gases such as He and H_2 can permeate small network pores. Therefore, an increase in $E_{P,\,He}$ and He selectivity indicates the densification of a network structure via condensation at high temperature [63]. As calcination temperature was increased, $E_{P,\,He}$ and He selectivities (He/N_2, He/H_2) were increased for BTESE and SiO_2 membranes. The network structures of BTESE and SiO_2 membranes were densified at high calcination temperatures. Moreover, $E_{P,\,He}$ and He selectivities of BTESE membranes were

comparable to that of SiO_2 membranes at 550 ºC. This suggests that a BTESE membrane calcined at 550 ºC develops a SiO_2-like network structure due to the pyrolysis of ethylene groups and a decrease in the proportion of carbon in the network structure.

BTESP membranes showed no apparent trend for increases in He selectivity as calcination temperature increased, and the selectivities were lower than those for BTESE and SiO_2 membranes at 350-700 ºC. Therefore, it seems reasonable to speculate that the BTESP membrane maintained a looser network structure regardless of calcination temperature. $E_{P,\ He}$ for the BTESP membrane was largely decreased at calcination temperatures ranging from 450 to 600 ºC, where a large weight loss was confirmed in TG-MS measurement, due to changes in the state of carbon.

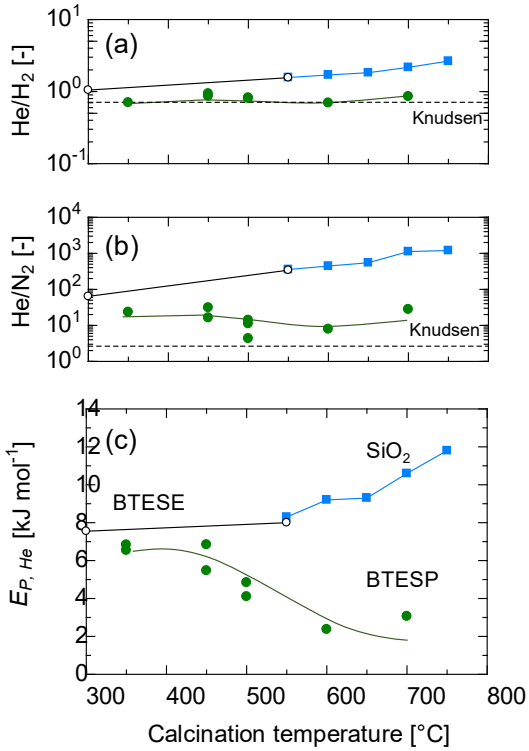

Fig. 13 He/H_2 selectivity (a), He/N_2 selectivity (b) at 200 ºC and activation energy for He permeation (c) as a function of calcination temperature for BTESP (AR = 10^{-1}), BTESE [47], and SiO_2 (TEOS) [62] membranes.

Activation energy and the H_2/N_2 permeance ratio were used to evaluate the effect that the membrane fabrication parameters, the acid molar ratio in the sol, and the calcination temperature exert on the network pore size. Fig. 14 shows the activation energy of He permeation and H_2/N_2 selectivity as a function of the activation energy of H_2 permeation for BTESP membranes calcined at 350 ºC with different ARs in the sol (a) and for membranes calcined at different temperatures with an AR = 10^{-1} (b). Activation energies and H_2/N_2 selectivity were decreased with increases in the acid molar ratio in the sol. BTESP membranes with a lower AR showed a particularly high activation energy of H_2 permeation that amounted to approximately 5-9 kJ mol^{-1} for the membrane with an AR = 10^{-2}, where H_2/N_2 selectivity was more than 20. Therefore, the AR of the sol is suitable for the tuning of small pore sizes. This is reasonable because small network pores can be formed by the condensation of Si-OH groups via the calcination process. In contrast, the activation energies and H_2/N_2 selectivity were decreased with increases in the calcination temperature, and produced activation energies of 1-3 kJ mol^{-1} and H_2/N_2 selectivities of 7-10 under high calcination temperatures (500-700 ºC). Calcination temperature as a membrane fabrication parameter offers the advantage of controllability in a loose network structure.

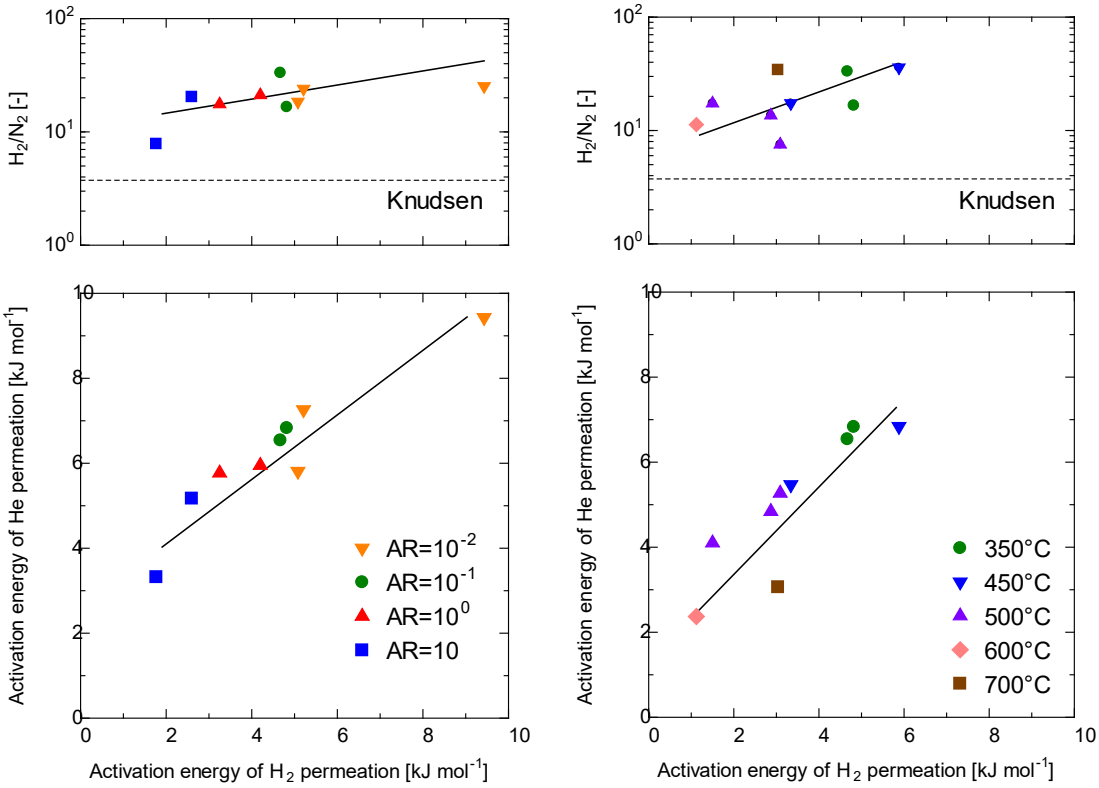

Fig. 14 Activation energy of He permeation as a function of the activation energy of H_2 permeation for BTESP membranes calcined at 350 °C with a different AR in the sol (a) and for membranes calcined at different temperatures with an AR = 10^{-1} (b).

4. Conclusions

Bis(triethoxysilyl)propane (BTESP) is a bridged-type organoalkoxysilane with a Si-C_3H_6-Si bond, and it was used for membrane fabrication via the sol-gel method. The effects that membrane fabrication parameters such as the acid molar ratio (HCl/Si, AR) and calcination temperature exerted on the network pore size and gas permeation properties were evaluated.

BTESP membranes with different ARs showed high H_2 permeance of approximately 1×10^{-6} mol m^{-2} s^{-1} Pa^{-1} with H_2/N_2 and H_2/CF_4 selectivities of 20-30 and 640-32000, respectively. Each gas permeance was increased with increases in the AR. H_2 selectivity, however, corresponded to the network pore size, and was decreased with a higher AR. The density of Si-OH groups (Si-OH/Si-O-Si) was decreased with a higher AR prior to the calcination process (condensation proceeded well with a high AR), so that many Si-OH groups were condensed during the calcination process when utilizing a sol with a low AR.

H_2 selectivity was decreased with higher calcination temperatures, since the linking units of BTESP were pyrolyzed at 500-700 ^oC under a N_2 atmosphere, and the state of carbon was changed from propylene groups to methyl groups by the higher calcination temperature.

Activation energies were decreased with increases in the AR in the sol. BTESP membranes with a lower AR showed a high activation energy of H_2 permeation that amounted to approximately 5-9 kJ mol^{-1} for the membrane with an AR = 10^{-2}. Therefore, the AR in a sol is considered suitable for the tuning of small pore sizes. In contrast, the activation energies were decreased with increases in the calcination temperature, which resulted in activation energies of 1-3 kJ mol^{-1} at high calcination temperatures (500-700 ^oC). Calcination temperature as a membrane fabrication parameter offers the advantage of controllability in a loose network structure.

References

[1] G.R. Gavalas, C.E. Megiris, S.W. Nam, Deposition of H_2-permselective SiO_2 films, Chem. Eng. Sci. 44 (1989) 1829-1835.

[2] S.S. Kim, B.K. Sea, Gas permeation characteristics of silica/alumina composite membrane prepared by chemical vapor deposition, Korean J. Chem. Eng. 18 (2001) 322-329.

[3] T. Yamaguchi, X. Ying, Y. Tokimasa, B.N. Nair, T. Sugawara, S. Nakao, Reaction control of tetraethylorthosilicate (TEOS)/O_3 and tetramethylorthosilicate (TMOS)/O_3 counter diffusion chemical vapor deposition for preparation of molecular-sieve membranes, Phys. Chem. Chem. Phys. 2 (2000) 4465-4469.

[4] S. Kitao, H. Kameda, M. Asaeda, Gas separation by thin porous silica membrane of ultra fine pores at high temperature, MAKU (Membrane) 15 (1990) 222-227.

[5] R.J.R. Uhlhorn, K. Keizer, A.J. Burggraaf, Gas transport and separation with ceramic membranes. Part II. Synthesis and separation properties of microporous membranes, J. Membr. Sci. 66 (1992) 271-287.

[6] I. Agirre, P.L. Arias, H.L. Castricum, M. Creatore, J.E. ten Elshof, G.G. Paradis, P.H.T. Ngamou, H.M. van Veen, J.F. Vente, Hybrid organosilica membranes and processes: status and outlook, Sep. Purif. Technol. 121 (2014) 2-12.

[7] G.J. Hwang, K. Onuki, S. Shimizu, H. Ohya, Hydrogen separation in H_2–H_2O–HI gaseous mixture using the silica membrane prepared by chemical vapor deposition, J. Membr. Sci. 162 (1999) 83-90.

[8] A.K. Prabhu, S.T. Oyama, Highly hydrogen selective ceramic membranes: application to the transformation of greenhouse gases, J. Membr. Sci. 176 (2000) 233-248.

[9] M. Asaeda, S. Yamasaki, Separation of inorganic/organic gas mixtures by porous silica membranes, Sep. Purif. Technol. (2001) 151-159.

[10] M.K. Koukou, N. Papayannakos, N.C. Markatos, M. Bracht, H.M. Van Veen, A.

Roskam, Performance of ceramic membranes at elevated pressure and temperature: effect of non-ideal flow conditions in a pilot scale membrane separator, J. Membr. Sci. 155 (1999) 241-259.

[11] R. Schafer, M. Noack, P. Kolsch, S. Thomas, A. Seidel-Morgenstern, J. Caro, Development of a H_2-selective SiO_2-membrane for the catalytic dehydrogenation of propane, Sep. Purif. Technol. 25 (2001) 3-9.

[12] T. Tsuru, K. Yamaguchi, T. Yoshioka, M. Asaeda, Methane steam reforming by microporous catalytic membrane reactors, AIChE J. 50 (2004) 2794-2805.

[13] M. Nomura, K. Ono, S. Gopalakrishnan, T. Sugawara, S.-I. Nakao, Preparation of a stable silica membrane by a counter diffusion chemical vapor deposition method, J. Membr. Sci. 251 (2005) 151-158.

[14] S. Chai, H. Du, Y. Zhao, Y. Lin, C. Kong, L. Chen, Fabrication of highly selective organosilica membrane for gas separation by mixing bis(triethoxysilyl)ethane with methyltriethoxysilane, Sep. Purif. Technol. 222 (2019) 162-167.

[15] H. R. Lee, T. Shibata, M. Kanezashi, T. Mizumo, J. Oshita, T. Tsuru, Pore-size-controlled silica membranes with disiloxane alkoxides for gas separation, J. Membr. Sci. 383 (2011) 152-158.

[16] G. Li, M. Kanezashi, T. Tsuru, Preparation of organic–inorganic hybrid silica membranes using organoalkoxysilanes: The effect of pendant groups, J. Membr. Sci. 379 (2011) 287-295.

[17] M. Kanezashi, R. Matsugasako, H. Tawarayama, H. Nagasawa, T. Tsuru, Pore size tuning of sol-gel-derived triethoxysilane (TRIES) membranes for gas separation, J. Membr. Sci. 524 (2017) 64-72.

[18] R.M. de Vos, W.F. Maier, H. Verweij, Hydrophobic silica membranes for gas

separation, J. Membr. Sci. 158 (1999) 277-288.

[19] M. Kanezashi, K. Yada, T. Yoshioka, T. Tsuru, Design of silica networks for development of highly permeable hydrogen separation membranes with hydrothermal stability, J. Am. Chem. Soc. 131 (2009) 414-415.

[20] M. Kanezashi, K. Yada, T. Yoshioka, T. Tsuru, Organic–inorganic hybrid silica membranes with controlled silica networks size: preparation and gas permeation characteristics, J. Membr. Sci. 348 (2010) 310-318.

[21] J. Campaniello, C.W.R. Engelen, W.G. Haije, P.P.A.C. Pex, J.F. Vente, Long-term pervaporation performance of microporous methylated silica membranes, Chem. Commun. (2004) 834-835.

[22] H.L. Castricum, A. Sah, J.A.J. Geenevasen, R. Kreiter, D.H.A. Blank, J.F. Vente, J.E. ten Elshof, Structure of hybrid organic–inorganic sols for the preparation of hydrothermally stable membranes, J. Sol–Gel Sci. Technol. 48 (2008) 11-17.

[23] H.L. Castricum, A. Sah, R. Kreiter, D.H.A. Blank, J.F. Vente, J.E. ten Elshof, Hybrid ceramic nanosieves: stabilizing nanopores with organic links, Chem. Commun. (2008) 1103-1105.

[24] H.L. Castricum, R. Kreiter, H.M. van Veen, D.H.A. Blank, J.F. Vente, J.E. ten Elshof, High-performance hybrid pervaporation membranes with superior hydrothermal and acid stability, J. Membr. Sci. 324 (2008) 111-118.

[25] H.L. Castricum, A. Sah, R. Kreiter, D.H.A. Blank, J.F. Vente, J.E. ten Elshof, Hydrothermally stable molecular separation membranes from organically linked silica, J. Mater. Chem. 18 (2008) 2150-2158.

[26] Q. Wei, F. Wang, Z. Nie, C. Song, Y. Wang, Q. Li, Highly hydrothermally stable microporous silica membranes for hydrogen separation, J. Phys. Chem. B 112 (2008)

9354-9359.

[27] R. Kreiter, M.D.A. Rietkerk, H.L. Castricum, H.M. van Veen, J.E. ten Elshof, J.F. Vente, Stable hybrid silica nanosieve membranes for the dehydration of lower alcohols, ChemSusChem 2 (2009) 158-160.

[28] Q. Wei, Y. Wang, Z. Nie, C. Yu, Q. Li, J. Zou, C. Li, Facile synthesis of hydrophobic microporous silica membranes and their resistance to humid atmosphere, Microporous Mesoporous Mater. 111 (2008) 97-103.

[29] M. Kanezashi, M. Kawano, T. Yoshioka, T. Tsuru, Organic-inorganic hybrid silica membranes with controlled silica network size for propylene/propane separation, Ind. Eng. Chem. Res. 51 (2012) 944-953.

[30] K.S. Chang, T. Yoshioka, M. Kanezashi, T. Tsuru, K.L. Tung, A molecular dynamics simulation of a homogeneous organic-inorganic hybrid silica membrane, Chem. Commun. 46 (2010) 9140-9142.

[31] K.S. Chang, T. Yoshioka, M. Kanezashi, T. Tsuru, K.L. Tung, Molecular simulation of micro-structures and gas diffusion behavior of organic-inorganic hybrid amorphous silica membranes, J. Membr. Sci. 381 (2011) 90-101.

[32] H.L. Castricum, G.G. Paradis, M.C. Mittelmeijer-Hazeleger, R. Kreiter, J.F. Vente, J.E. ten Elshof, Tailoring the separation behavior of hybrid organosilica membranes by adjusting the structure of the organic bridging group, Adv. Funct. Mater. 21 (2011) 2319-2329.

[33] H.W. Oviatt, K.J. Shea, J.H. Small, Alkylene-bridged silsesquioxane sol-gel synthesis and xerogel characterization. Molecular requirements for porosity, Chem. Mater. 5 (1993) 943-950.

[34] R. Xu, M. Kanezashi, T. Yoshioka, T. Okuda, J. Ohshita, T. Tsuru, Tailoring the

affinity of organosilica membranes by introducing polarizable ethenylene bridges and aqueous ozone modification, ACS Appl. Mater. Interfaces 5 (2013) 6147-6154.

[35] R. Xu, P. Lin, Q. Zhang, J. Zhong, T. Tsuru, Development of ethenylene-bridged organosilica membranes for desalination applications, Ind. Eng. Chem. Res. 55 (2016) 2183-2190.

[36] A. P. Dral, J.E. ten Elshof, Organic groups influencing microporosity in organosilicas, Micropor. Mesopor. Mat. 267 (2018) 267-273.

[37] X. Ren, K. Nishimoto, M. Kanezashi, H. Nagasawa, T. Yoshioka, T. Tsuru, CO_2 permeation through hybrid organosilica membranes in the presence of water vapor, Ind. Eng. Chem. Res. 53 (2014) 6113-6120.

[38] M. Kanezashi, Y. Yoneda, H. Nagasawa, T. Tsuru, K. Yamamoto, J. Ohshita, Gas permeation properties for organosilica membranes with different Si/C ratios and evaluation of microporous structures, AIChE J. 63 (2017) 4491-4498.

[39] T. Tsuru, N. Moriyama, H. Nagasawa, M. Kanezashi, Nano/subnano-tuning of Porous Silica Membranes and Application to Hydrogen Separation, MAKU (Membrane) 43 (2018) 180-187.

[40] T. Niimi, H. Nagasawa, M. Kanezashi, T. Yoshioka, K. Ito, T. Tsuru, Preparation of BTESE-derived organosilica membranes for catalytic membrane reactors of methylcyclohexane dehydrogenation, J. Membr. Sci. 455 (2014) 375-383.

[41] S. M. Ibrahim, H. Nagasawa, M. Kanezashi, T. Tsuru, Organosilica bis(triethoxysilyl)ethane (BTESE) membranes for gas permeation (GS) and reverse osmosis (RO): The effect of preparation conditions on structure, and the correlation between gas and liquid permeation properties, J. Membr. Sci. 526 (2017) 242-251.

[42] H. L Castricum, H. F. Qureshi, A. Nijmeijer, L. Winnubst, Hybrid silica membranes

with enhanced hydrogen and CO_2 separation properties, J. Membr. Sci. 488 (2015) 121-128.

[43] N. Moriyama, H. Nagasawa, M. Kanezashi, K. Ito, T. Tsuru, Bis(triethoxysilyl)ethane (BTESE)-derived silica membranes: pore formation mechanism and gas permeation properties, J. Sol–Gel Sci. Technol. 86 (2018) 63-72.

[44] G. Cao, Y. Lu, L. Delattre, C.J. Brinker, G. P. Lopez, Amorphous silica molecular sieving membranes by sol-gel processing, Adv. Mater. 8 (1996) 588-591.

[45] K. Kusakabe, S. Sakamoto, T. Saie, S. Morooka, Pore structure of silica membranes formed by a sol-gel technique using tetraethoxysilane and alkyltriethoxysilanes, Sep. Purif. Technol. 16 (1999) 139-146.

[46] G. Xomeritakis, S. Naik, C.M. Braunbarth, C.J. Cornelius, R. Pardey, C.J. Brinker, Organic-templated silica membranes I. Gas and vapor transport properties, J. Membr. Sci. 215 (2003) 225-233.

[47] X. Yu, H. Nagasawa, M. Kanezashi, T. Tsuru, Improved thermal and oxidation stability of bis(triethoxysilyl)ethane (BTESE)-derived membranes, and their gas-permeation properties, J. Mater. Chem. A 6 (2018) 23378-23387.

[48] Y.H. Han, A. Taylor, M. D. Mantle, K. M. Knowles, Sol-gel-derived organic-inorganic hybrid materials, J. Non-Cryst. Solids 353 (2007) 313-320.

[49] B. Cao, Y. Tang, C. Zhu, Z. Zhang, Synthesis and hydrolysis of hybridized silicon alkoxide: $Si(OEt)_x(OBut)_{4-x}$. Part I: synthesis and identification of the $Si(OEt)_x(OBut)_{4-x}$, J. Sol–Gel Sci. Technol. 10 (1997) 247-253.

[50] Y. Liang, R. Anwander, Synthesis of pore-enlarged mesoporous organosilicas under basic conditions, Microporous Mesoporous Mater. 72 (2004) 153-165.

[51] M. A.Wahab, II. Kim, C.-S. Ha, Hybrid periodic mesoporous organosilica materials

prepared from 1,2-bis(triethoxysilyl)ethane and (3-cyanopropyl)triethoxysilane, Microporous Mesoporous Mater. 69 (2004) 19-27.

[52] G. Das, P. Bettotti, L. Ferraioli, R. Raj, G. Mariotto, L. Pavesi, G. D. Sorarùa, Study of the pyrolysis process of an hybrid $CH_3SiO_{1.5}$ gel into a SiCO glass, Vibrational Spectroscopy 45 (2007) 61-68.

[53] H. Ishida, J. Koenig, Fourier transform infrared spectroscopic study of the silane coupling agent/porous silica interface, J. Colloid Interface Sci. 64 (1978) 555-564.

[54] A. Shimojima, K. Kuroda, Designed synthesis of nanostructured siloxane–organic hybrids from amphiphilic silicon-based precursors, Chem. Rec., 6 (2006) 53-63.

[55] B. Boury, R.J.P. Corriu, Auto-organisation of hybrid organic–inorganic materials prepared by sol–gel process, Chem. Commun. (2002) 795-802.

[56] M. JafarzadehI, A. Rahman, C. S. Sipaut, Synthesis of silica nanoparticles by modified sol–gel process: the effect of mixing modes of the reactants and drying techniques, J. Sol–Gel Sci. Technol. 50 (2009) 328-336.

[57] D. A. Loy, G. M. Jamison, B. M. Baugher, E. M. Russick, R. A. Assink, S. Prabaker, K. J. Shea, Alkylene-bridged polysilsesquioxane aerogels: highly porous hybrid organic-inorganic materials, J. Non-Cryst. Solids 186 (1995) 44-53.

[58] G. Caminoa, S.M. Lomakin, M. Lageard, Thermal polydimethylsiloxane degradation. Part 2. The degradation mechanisms, Polymer 43 (2002) 2011-2015.

[59] K. Maeda, Y. Mito, T. Yanagase, S. Haraguchi, T. Yamazaki, T. Suzuki, The first synthesis of organosilyl-substituted aluminophosphate molecular sieves, Chem. Commun. (2007) 283-285.

[60] H. Inde, M. Kanezashi, H. Nagasawa, T. Nakaya, T. Tsuru, Tailoring a thermally stable amorphous SiOC structure for the separation of large molecules: the effect of

calcination temperature on SiOC structures and gas permeation properties, ACS OMEGA 3 (2018) 6369-6377.

[61] H. EI Rassy, A.C. Pierre, NMR and IR spectroscopy of silica aerogels with different hydrophobic characteristics, J. Non-Crystaline Solids. 351 (2005) 1603-1610.

[62] M. Kanezashi, T. Sasaki, H. Tawarayama, H. Nagasawa, T. Yoshioka, K. Ito, T. Tsuru, Experimental and theoretical study on small gas permeation properties through amorphous silica membranes fabricated at different temperatures, J. Phys. Chem. C 118 (2014) 20323-20331.

[63] M. Kanezashi, T. Sasaki, H. Tawarayama, T. Yoshioka, T. Tsuru, Hydrogen permeation properties and hydrothermal stability of sol-gel-derived amorphous silica membranes fabricated at high temperatures, J. Am. Ceram. Soc. 96 (2013) 2950-2957.